Nano Energy 34 (2017) 120–130

Contents lists available at ScienceDirect

Nano Energy

journal homepage: www.elsevier.com/locate/nanoen

Full paper

Highly stable $Li_{1.2}Mn_{0.54}Co_{0.13}Ni_{0.13}O_2$ enabled by novel atomic layer deposited $AlPO_4$ coating

Biwei Xiao[a,b,1], Biqiong Wang[a,c,1], Jian Liu[a], Karthikeyan Kaliyappan[a], Qian Sun[a], Yulong Liu[a], Gayatri Dadheech[b], Michael P. Balogh[b], Li Yang[b], Tsun-Kong Sham[c], Ruying Li[a], Mei Cai[b,*], Xueliang Sun[a,*]

[a] Department of Mechanical and Materials Engineering, University of Western Ontario, London, Ontario, Canada N6A 6B9
[b] General Motors Research & Development Center, Warren, MI 48090-9055, Unites States
[c] Department of Chemistry, University of Western Ontario, London, ON, Canada N6A 5B7

ARTICLE INFO

Keywords:
Li-rich NMC
Atomic layer deposition
Aluminum phosphate
X-ray absorption spectroscopy
Coulombic efficiency
Lithium-ion batteries

ABSTRACT

Lithium-rich layered material is one of the most promising candidates of cathode materials for next-generation electric vehicles. However, one of the major issues that pertains to this material is the oxygen release during initial charge, which results in low initial coulombic efficiency (CE), intense electrolyte oxidation and thermal instability. In this study, we have conducted aluminum phosphate ($AlPO_4$) coating *via* atomic layer deposition (ALD) approach to protect the surface of this cathode material powders. It was found that part of the C2/m Li_2MnO_3 phase turned into a spinel-like phase during the ALD process. The oxygen release has been effectively suppressed by such transformation, the initial CE increased from 75.2% for the bare electrode to 86.2% for the electrode with only 5 ALD cycles of $AlPO_4$ coating. Furthermore, $AlPO_4$ was also found to be more effective in improving the thermal stability of the cathode material comparing to bare or Al_2O_3 coated samples. Our study has provided a new possible solution towards cathode materials with high thermal resistance *via* conformal coating.

1. Introduction

Lithium-rich layered oxides $xLi_2MnO_3 \bullet (1-x)LiMO_2$ (M = Mn, Ni, Co), or otherwise termed as high energy NMC (HENMC) are a class of cathode materials that deliver a discharge capacity higher than 250 mAh/g within the voltage window of 2.0–4.8 V (vs. Li/Li^+), making it a very promising cathode material for the next-generation high energy lithium-ion batteries (LIBs) used in electric vehicles (EV) [1,2]. The crystalline structure of HENMC is composed of a phase of Li_2MnO_3 with a space group of C2/m and a phase of conventional layered $LiMO_2$ (M = Ni, Mn, Co) with a space group of R $\bar{3}$m. Li_2MnO_3 is electrochemically inert since Mn^{4+} cannot be oxidized any more under the normal operating voltage range of conventional LIBs. It can, however, be activated from the initial charging process by the simultaneous leaching of Li^+ from the transition metal layer and O_2 from the lattice, with an irreversible net loss of Li_2O [3,4]. The initial activation process of HENMC results in significantly increased capacity compared to other layered structure cathode materials, but it also leads to several disadvantages. Firstly, the transition metal ions move into the Li layer vacancies and cause subsequent cation disordering, forming a spinel and then rock-salt phase continuously to the interior of the material that will lead to sluggish lithium ions transportation and severe voltage fade [5,6]. Secondly, O_2 release results in low initial CE and internal pressure increase in the cell, furthermore, O_2 facilitates the oxidation of the electrolyte under high voltage, forming a thick and insulating solid electrolyte interphase (SEI) on the surface [7]. Thirdly, O_2 release always gives rise to thermal instability of the cathode materials [8,9]. Fourthly, severe transition metal dissolution into the electrolyte also leads to capacity fade. Surface coating with metal oxides, phosphates and fluorides from chemical methods have been reported aimed at solving the abovementioned problems [10–12]. The coating layer can shield the direct contact between the cathode material and the electrolyte and thus preventing the transition metals from dissolving and electrolyte decomposition [13]. But these coating methods lack a full protection of the cathode materials since the coating layer tends to form isolated islands [12,14,15]. Atomic layer deposition (ALD) is a powerful technique to create a uniform and conformal coating layer on the surface of substrates [16]. This advantage makes ALD outperform

* Corresponding authors.
E-mail addresses: mei.cai@gm.com (M. Cai), xsun@eng.uwo.ca (X. Sun).
[1] These authors contributed equally to this paper.

http://dx.doi.org/10.1016/j.nanoen.2017.02.015
Received 13 January 2017; Received in revised form 10 February 2017; Accepted 10 February 2017
Available online 13 February 2017

other chemical methods in terms of full protection on electrodes against the attack from the electrolytes, and it has been vastly used in the surface modification of battery materials [17–20]. Aluminum phosphate (AP) is widely known for its high capability of enhancing the high temperature stability of cathode materials than metal oxides when used as a coating material [21–24], but controlled coating of AP *via* ALD on cathode materials has not been reported as far.

Herein, for the first time, we have demonstrated the use of ALD to coat cathode materials with different thicknesses of $AlPO_4$. Benefiting from the uniform coating layer and the partial transformation of Li_2MnO_3 to a spinel-like phase, the oxygen release from the HENMC has been successfully controlled and the electrolyte decomposition was suppressed. The CE of the HENMC coated by $AlPO_4$ was significantly improved. In addition, the $AlPO_4$ coated HENMC has demonstrated much higher thermal resistivity than samples coated by Al_2O_3, which is a most common ALD coating material. These results have demonstrated that atomic layer deposited $AlPO_4$ is a promising coating material on HENMC in order to achieve better cycling stability and that ALD process can potentially affect the structure of cathode materials.

2. Experimental section

2.1. Materials synthesis

HENMC was synthesized using a modified Pechini's method [25]. CH_3COOLi, $Mn(CH_3COO)_2$, $Ni(CH_3COO)_2$ and $Co(CH_3COO)_2$ (Sigma Aldrich, 99%) were mixed with a stoichiometric ratio of 1.25:0.54:0.13:0.13 in 50 mL deionized water under strong stirring. 5.72 g citric acid was dissolved in 25 mL ethanol (Sigma Aldrich, 99.99%). 2.5 g polyethylene glycol (PEG) (Alfa Aesar, 25,000, 99%) was dissolved in 25 mL ethanol separately. The citric acid solution was initially added into the metal acetates solution slowly under stirring for 10 min. Then, the mixture was subsequently added into the PEG solution slowly, pink precipitations were observed during the reaction. Subsequently, 2 mL ethylene glycol (Sigma Aldrich, 99%) and 2 mL HNO_3 (Sigma Aldrich, 70%) were added dropwise until the pink precipitate is dissolved. The final clear solution was dried at 120 °C to obtain a colloidal gel. This gel was pre-calcined at 400 °C for 4 h in air to remove the organic components. After cooling down, the final product was collected and ground to obtain fine particles. The final HENMC was obtained by calcining the fine particles under 850 °C for 20 h in air.

$AlPO_4$ was deposited on HENMC powders at 250 °C in a Savannah 100 ALD system (Ultratech/Cambridge Nanotech, USA) using trimethylaluminum (TMA, $(CH_3)_3Al$, 98% STREM Chemicals), trimethyl phosphate (TMPO, $(CH_3)_3PO_4$, 97% STREM Chemicals), and distilled water (H_2O) as precursors. The source temperature for TMPO was 75 °C, while TMA and H_2O was kept at RT. $AlPO_4$ was deposited in an exposure model by the sequence of TMA pulse (0.5s) – exposure (1s) - purge (10s) – H_2O pulse (1s) – exposure (1s) – purge (15s) – TMPO pulse (2s) – exposure (1s) – purge (10s) – H_2O pulse (1s) – exposure (1s) – purge (10s). Nitrogen gas (99.999%) was used as a carrier gas at a flow rate of 20 sccm. $AlPO_4$ films were directly deposited on HENMC powders by repeating the above ALD cycles. In this study, 5, 10 and 20 ALD cycles were selected to control the coating thickness, each of the sample was denoted as HENMC-*n* AP, where *n* stands for the ALD cycle number and AP stands for $AlPO_4$. In addition, for the purpose of thermal stability comparison, Al_2O_3 coating with 20 ALD cycles on the HENMC was carried out at 150 °C with TMA and water as the precursors in the same ALD system.

2.2. Characterization methods

The morphology of the samples was characterized by a Hitachi S-4800 field emission scanning electron microscopy (FESEM) and a JEOL 2010F high-resolution transmission electron microscope (HRTEM). The stoichiometry of the HENMC powders was determined by an inductively coupled plasma optical emission spectrometer (ICP-OES, Vista Pro Axial, Varian, Australia) The X-ray diffraction (XRD) patterns were collected on a Bruker D8 Advance Diffractometer using Cu K_α radiation at 40 kV and 40 mA. The soft X-ray absorption spectroscopy (XAS) measurements of P $L_{3,2}$ edges were collected at the Variable Line Spacing Plane Grating Monochromator (VLS PGM) beamline with a photon energy of 5.5–250 eV at the Canadian Light Source (CLS). The soft X-ray absorption spectroscopy (XAS) measurements at both total electron yield (TEY) and fluorescence yield (FYI) modes of Mn $L_{3,2}$ edges, Ni $L_{3,2}$ edges, Co $L_{3,2}$ edges and O K edge were collected at the Spherical Grating Monochrometer (SGM) beamline with a photon energy of 250–2000 eV at CLS. A PHI Quantera XPS Scanning Microprobe (Physical Electronics, Chanhassen, MN) with a monochromated Al K_α (1486.6 eV) source was used for the XPS analysis. Differential scanning calorimetry (DSC) measurements were carried out on a TA Instrument SDT Q600. The cells were cycled for 5 times and stopped at fully charged state and were opened in the glovebox to collect the fully de-lithiated cathode powders. The powders were then soaked in 150 mg of the same electrolyte as the electrochemical study and heated to 400 °C under N_2 atmosphere at a ramp rate of 1 °C/min.

2.3. Electrochemical measurements

To prepare the electrodes for coin cell fabrication, the HENMC powders were uniformly mixed with acetylene black (AB) and poly(-vinylidene fluoride) (PVDF) in a ratio of 70:20:10 in an N-methyl-pyrrolidione (NMP) solvent. Then, the slurry was pasted on aluminum foils and dried at 80 °C under vacuum for overnight. The electrode was subsequently punched and assembled into a CR-2032 coin cell in an argon-filled glove box with the moisture and oxygen being controlled below 0.1 ppm. Lithium metal was used as the counter electrode in the coin cells. One mole/L $LiPF_6$ dissolved into ethylene carbonate (EC) and diethyl carbonate (DEC) in a 1:1 vol ratio (BASF corp., US) was used as the electrolyte. Celgard 2400 was used as the separator. Cyclic voltammetry (CV) was performed on a Bio-Logic multichannel potentiostat 3/Z (VMP3) with a scanning rate of 0.1 mV s^{-1} and a potential range of 2.0–4.6 V (vs Li/Li^+). Galvanostatical charge/discharge test was carried out on Maccor 4000 between 2.0 V and 4.6 V (vs Li/Li^+), the initial cycle was conducted under 1/20 C (12.5 mA/g) for activation, and the following cycles were tested under 1/10 C (25 mA/g). The tested cells were dissembled in a glove box and the cathode sheets were collected and thoroughly washed with DMC several times for XPS analysis.

3. Results and discussions

The stoichiometry of the as-synthesized HENMC powders was determined by ICP, the ratio between the transition metals was found to be Co:Mn:Ni =0.137:0.540:0.135, which agrees well with the original stoichiometry during synthesis. The SEM image of the HENMC particles is shown in Fig. 1a-b, the uniform nanoparticles have sizes of around 300 nm. The smooth face and sharp edges indicate that the HENMC was crystalline and highly interconnected, which is essential for faster ionic transportation. The morphology of the HENMC-20AP shown in Fig. 1b displays a slightly rougher surface, indicating that the surface has been coated by $AlPO_4$. The XRD pattern of the HENMC (Fig. 1c) was well indexed to the hexagonal α-$NaFeO_2$ phase with a space group of R $\bar{3}$m. The weak peaks located between 20 and 25° are assigned to the superlattice diffraction of the monoclinic Li_2MnO_3 phase with a space group of C2/m, as can be observed in its standard XRD patterns. The presence of the amorphous $AlPO_4$ did not generate significant change to the XRD pattern, indicating that the bulk of the material remains unchanged. Nevertheless, the surface structure

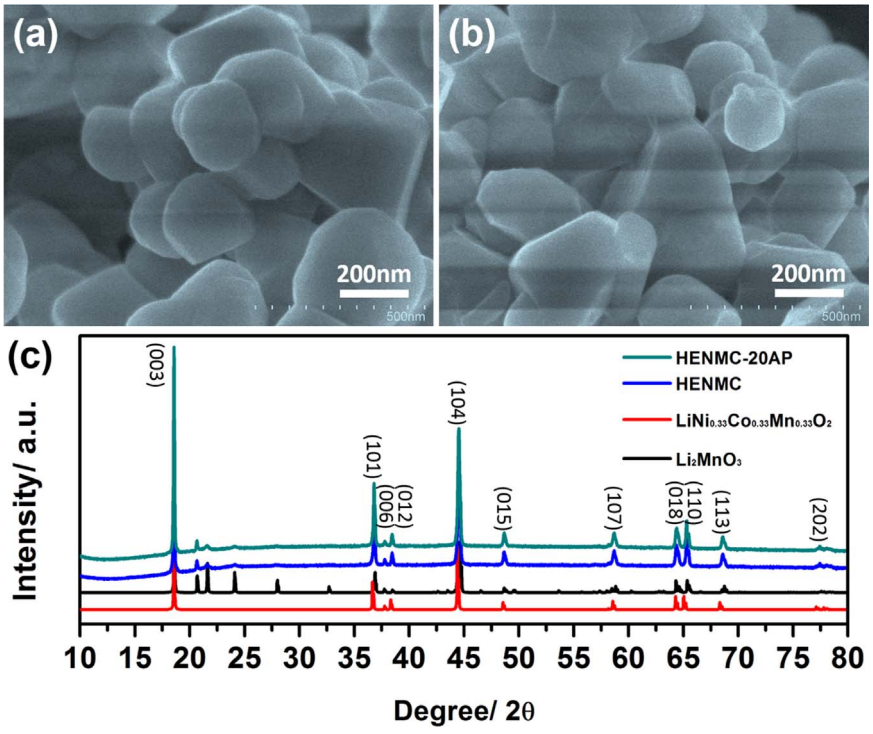

Fig. 1. SEM images of (a) HENMC (b) HENMC-20AP and (c) XRD patterns of HENMC, HENMC-20AP and standard Li_2MnO_3 and $LiNi_{0.33}Co_{0.33}Mn_{0.33}O_2$.

change needs to be identified by other techniques aimed at probing the local structures, which will be carried out in following discussions.

The elemental distribution of the HENMC-20AP sample was studied using energy dispersive X-ray spectroscopy (EDS) under the scanning transmission electron microscopy (STEM) mode. Fig. 2a-f present the distribution of Co, Mn, Ni, Al, P elements and the overlapping mapping of Al and P. It can be seen that the Al and P are uniformly distributed on the surface of the HENMC particles. The inset P $L_{3,2}$ edges X-ray absorption spectroscopy (XAS) in Fig. 2g reveals that the ALD derived $AlPO_4$ has very close chemical environment with standard $AlPO_4$. The Al $L_{3,2}$ edges XAS shown in Fig. S1 also proves its presence. The HRTEM image reveals that the thickness of the 20 AP sample is around 4 nm and the $AlPO_4$ coating layer is amorphous and uniformly distributed on the surface of the powders.

The Ni, Mn and Co $L_{3,2}$ edges and O K edge XAS data of the pristine HENMC and 20AP coated HENMC was collected in order to study the local chemical environment change upon ALD process. Fig. 3a-e illustrate the total electron yield (TEY) mode results, which have a detection depth of 5–10 nm. Transition meal $L_{3,2}$ edges reveal the electron transition of $2p_{3/2}$ and $2p_{1/2}$ states to an unoccupied *3d*

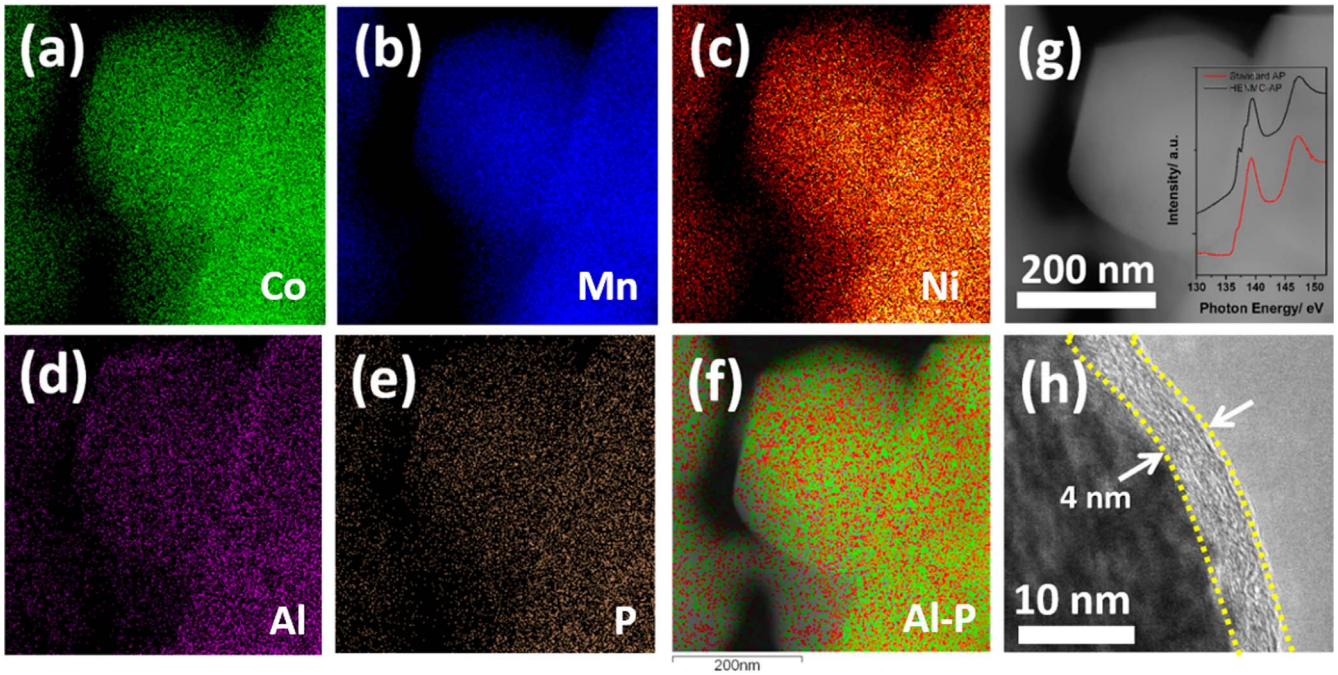

Fig. 2. (a-f) EDS mapping of Co, Mn, Ni, Al, P and Al-P overlapping of HENMC-20AP (g) STEM image of the EDS mapping region (inset: XAS spectra of P $L_{3,2}$ edges of HENMC-AP (Black) and standard $AlPO_4$ (Red)) and (h) HRTEM image of the HENMC-20AP showing the coating layer.

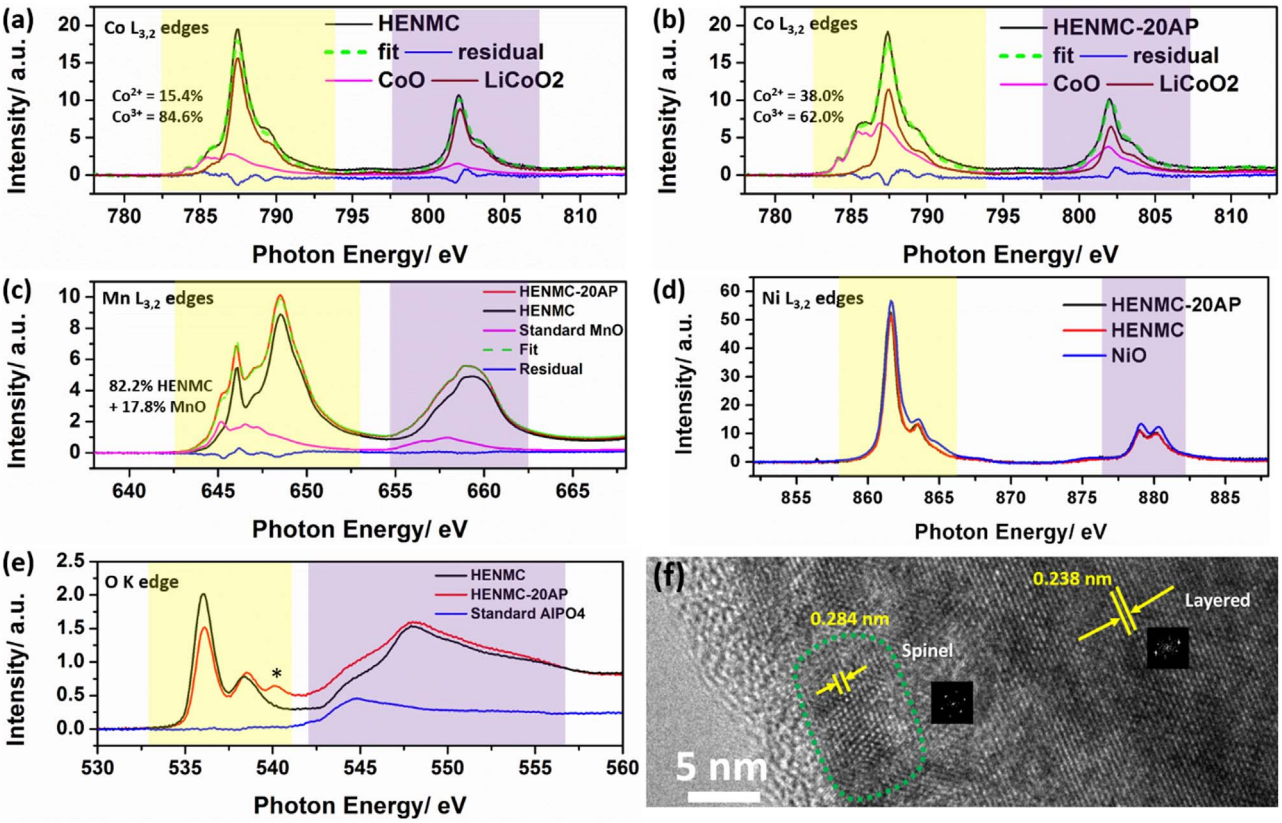

Fig. 3. Soft XAS data of (a) HENMC Co $L_{3,2}$ edges and (b) HENMC-20AP Co $L_{3,2}$ edges fitted to standard CoO and $LiCoO_2$ (c) Mn $L_{3,2}$ edges (the HENMC-20AP sample is fitted to the HENMC sample and standard MnO) (d) Ni $L_{3,2}$ edges (L_3 edges are marked with yellow color and L_2 edges are marked with purple color) (e) O K edge (all of the XAS results in this figure are collected at total electron yield (TEY) mode) and (f) HRTEM image showing the different phases in the HENMC-20AP sample (inset: Fast Fourier Transform patterns).

state, and thus can provide information of spin configuration, ligand field and metal valence [26]. The Co $L_{3,2}$ edges of these two samples were fitted using a linear combination fitting method with standard CoO (divalent Co) and $LiCoO_2$ (trivalent Co) respectively in order to understand the Co valence states. Fig. 3a shows the fitted result of the pristine HENMC, it can be seen that the Co ions in the pristine HENMC are composed of 15.4% divalent Co and 84.6% trivalent Co. After ALD treatment, however, an increase in the ratio of Co^{2+} occurred, and the trivalent Co dropped to only 62%. The decrease of Co^{3+} amount in the HENMC-20AP sample reveals that the surface of the HENMC was reduced upon ALD treatment. The reduction was also observed in the Mn $L_{3,2}$ edges. Since Mn $L_{3,2}$ edges of the HENMC sample were very hard to fit using MnO_2, Mn_2O_3 and MnO, we used the Mn $L_{3,2}$ edges of the HENMC directly and MnO as standards to fit the HENMC-20AP sample. The results clearly show that the surface of the HENMC-20AP sample had 17.8% Mn existing in divalent state and only 82.2% in the original form of Mn in HENMC. In contrast to the Mn and Co, Ni did not show any change in the coated sample. O K edge shows several identical peaks, the peaks in yellow and purple regions are due to electron transition from the O *1s* core level to the hybridization of the O *2p* orbital with the transition metal *3d* and *4sp* orbitals, respectively [27]. An intensity drop happened on the sample after ALD process in the yellow region due to less electron holes, this complies with the finding of transition metal reduction [26]. On the other hand, the new peak marked with an asterisk "*" indicates that a TM-O ligand with different environment has evolved, which also suggests that a different phase formed on the surface. XAS results measured under fluorescence yield (FYI) mode with a depth of up to 100 nm [28] are shown in Fig. S2, the two samples do not show much difference, indicating that the effect of ALD process only happens on the surface, which agrees well with the XRD results. Raman spectra in Fig. S4 proves the presence of this spinel phase as can be seen from the extra peak at higher wave number. In fact, the surface reduction of Li-rich material when exposed to hydrazine and carbon has been reported by other groups [29,30], they found that a spinel phase formed as a result of this reduction. Such spinel phase differs from the spinel-like phase formed after cycling, where Li vacancy in the lithium layer was the reason and it caused continuous growth to the interior particle. Cho et al. investigated the formation of a *Fd* $\bar{3}m$ $Li_{1+x}[CoNiMn_{2-x}]_2O_4$ spinel phase on a R $\bar{3}$m $Li[Ni_{0.54}Co_{0.12}Mn_{0.34}]O_2$ layered phase and found that such transition was accompanied with oxygen loss, which is reflected as transition metal reduction in order to keep the charge balance [31]. To better understand the possible phase change in our samples, HRTEM images on the surface region of a HENMC-20AP sample particle were collected. As shown in Fig. 3f, two distinctive phases are observed. The one in the deeper region has a spacing of 0.238 nm, and can be indexed to the (113) crystalline plane of a typical layered R $\bar{3}$m phase. Interestingly, a spinel phase with a spacing of 0.284 nm on the surface can be observed. Combined with the XAS data, we conclude that the surface spinel phase formed upon ALD treatment. In this case, it is believed that the HENMC particles reacted with the ALD precursors and formed such spinel structure while $AlPO_4$ was deposited. This transformation was also observed in AlF_3 coating reported by Scrosati et. al, it was attributed to the Li^+ leaching from the Li_2MnO_3 phase [32]. In previous ALD-related surface modification studies, not many evidences were provided to the structural change upon the ALD process. Therefore, we expect that in future, the effect would be studied more with respect to the structural changes due to ALD process, though the coating layer also plays a pivotal role.

Initially, the CV curves of the pristine HENMC and the HENMC coated with various ALD cycles of AP were recorded at 0.1 mVs^{-1} scan rate within 2.0–4.6 V and the results are illustrated in Fig. 4. In a typical HENMC CV profile, the anodic peak at around 4.1 V corresponds to the oxidation of Ni^{2+} to Ni^{4+}. Another sharp anodic peak at

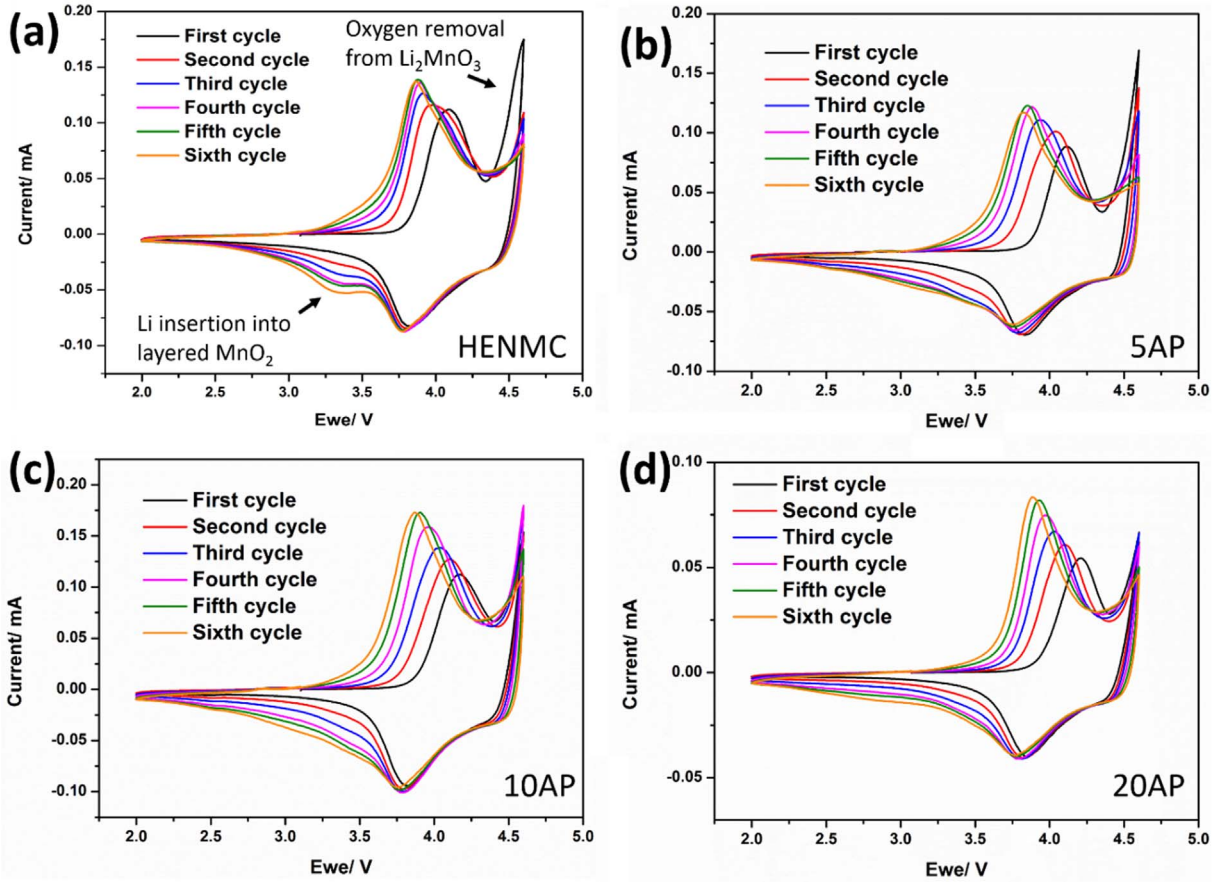

Fig. 4. Cyclic voltammetry of (a) pristine HENMC (b) HENMC-5AP (c) HENMC-10AP (d) HENMC-20AP.

4.5 V is attributed to the removal of oxygen from the crystal structure and formation of O_2^{2-} or O_2, which are distinctive resultants of the activation of the Li_2MnO_3 phase [4]. In the following cathodic process, the peak at around 3.8 V corresponds to the reduction of Ni^{4+} to Ni^{2+} [5,33]. In general, it is believed that the Li_2MnO_3, after the Li_2O net loss, turns into layer-structured MnO_2 [5], which is capable of accommodating lithium ions at the potential of ~ 3.5 V. This is consistent with what was observed from the pristine HENMC CV curve, that a peak increases gradually at ~3.25 V with continuous cycle numbers. Interestingly, the AP coated samples show significant difference compared to the pristine sample. The oxygen formation peak intensity has dropped gradually with more ALD cycles, indicating that the amount of the Li_2MnO_3 phase has dropped with ALD treatment and the coating thickness of AP correlates with the degree of oxygen removal from the HENMC. This observation complies with the XAS study, that the surface Li_2MnO_3 phase has been changed upon ALD process. The decreasing cathodic current peak of lithium insertion into layered MnO_2 also confirms the controlled oxygen removal since they form simultaneously. Though the spinel phase was only observed on the surface, CV tests shows remarkable effect.

In order to evaluate the electrochemical performance of the samples, charge/discharge measurements were conducted with one activation cycle at 1/20 C and another 39 cycles at 1/10 C rate, the result is shown in Fig. 5a. The initial charge capacity, discharge capacity and CE are listed in Table 1. The pristine HENMC delivers an initial charge capacity of 327 mAh/g, which decreases with thicker coating. The initial discharge capacity of the pristine HENMC is only 249 mAh/g, which is lower than those of the coated samples. Interestingly, the capacity of the HENMC drops rapidly after 40 cycles, whereas those of the coated samples remain rather stable, and an increase of capacity can even be observed in the first several cycles.

The CE is plotted in Fig. 5b. The pristine HENMC has an initial CE of only 76.1%, whereas the coated HENMC samples demonstrate initial CEs of 85.2%, 84.1% and 83.2% for 5 AP, 10 AP and 20 AP, respectively. Due to the loss of active MnO_2, the discharge capacities of the HENMC-10AP and HENMC-20AP samples are lower than that of the HENMC-5AP sample. This explains why the initial CE drops with increasing coating thickness while 5 ALD cycles demonstrates the highest CE. Furthermore, the low initial CE normally results from the electrolyte decomposition and the oxygen release in the class of lithium-rich cathode materials [2]. As observed and discussed in the CV curves (Fig. 4), the suppression of oxygen release has been well controlled by the process of ALD treatment, this would account for the increase of initial CE as well. On the other hand, the release of oxygen will certainly facilitate the decomposition of the electrolyte under high voltage and it inevitably brings another consideration, that the solid electrolyte interphase (SEI) on the HENMC surface becomes very thick and results in impedance build-up, thereby the pristine HENMC shows decreasing stability upon cycling.

As has been introduced, the voltage fade issue is an important concern in lithium-rich cathodes since it causes energy density drop, and the reason for the voltage fade is still under debate. One possible explanation is the migration of transition metals into the Li vacancies in the Li layer during charging, resulting in the formation of a spinel phase on the surface. The average voltage for this spinel phase is lower than that of the layered NMC, therefore the overall voltage drops [6,34,35]. In order to analyze the effect of AP coating on the voltage fade of HENMC materials, the charge/discharge curves of the first and 40th cycles are plotted and illustrated in Fig. 5c. In a typical HENMC charge curve, the voltage range of 3.7–4.5 V corresponds to the lithium de-lithiation from the NMC phase, and the long plateau at 4.5–4.6 V can be assigned to the oxygen release from the lattice. The oxygen

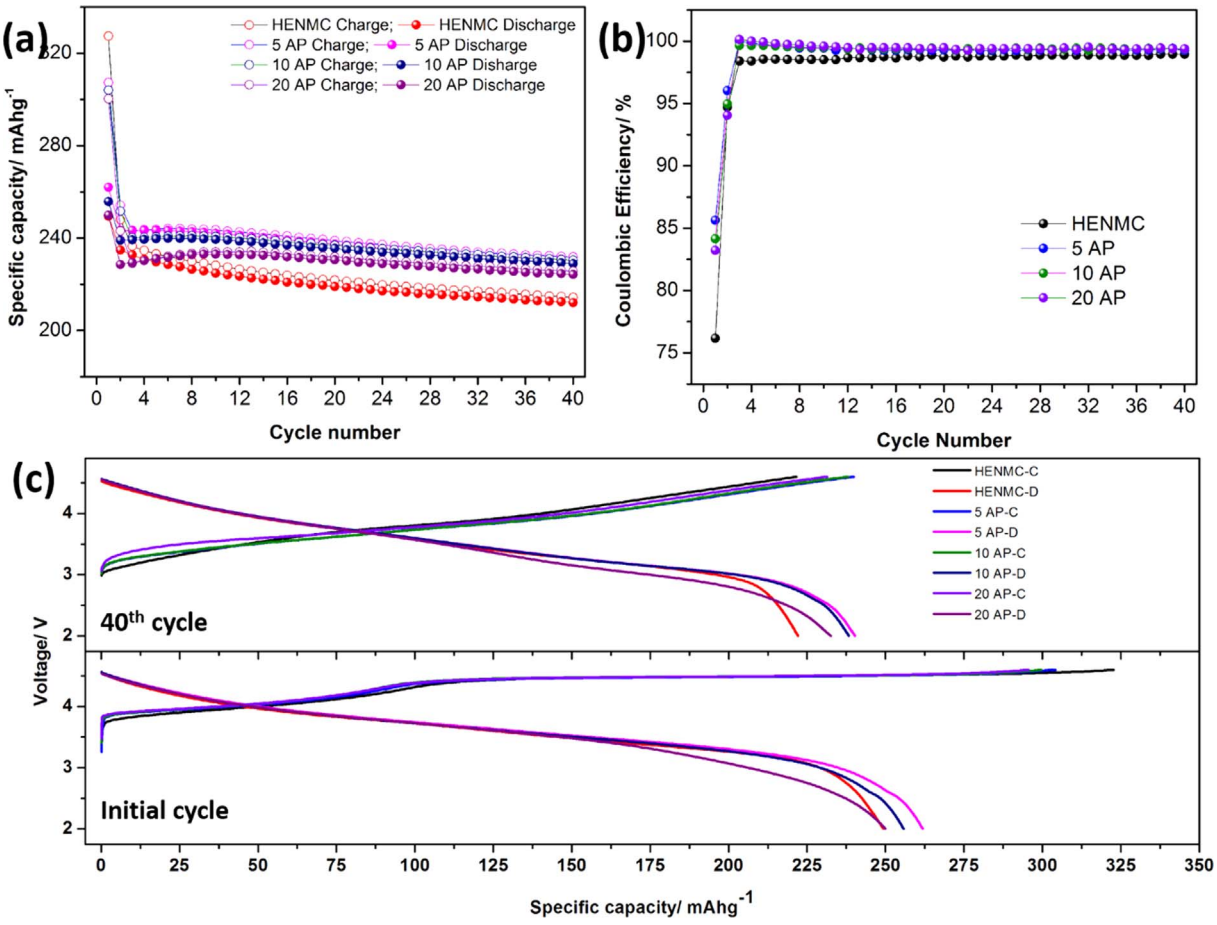

Fig. 5. (a) Cyclic stability performance; (b) Coulombic efficiencies; (c) First cycle charge/discharge curves and 40th cycle charge/discharge curves of the samples.

Table 1
Initial charge/discharge capacity and the Coulombic efficiencies of the samples.

Sample name	Initial charge capacity (mAh/g)	Initial discharge capacity (mAh/g)	Initial CE (%)
HENMC	327.4	249.4	76.2
5 AP	307.3	261.9	85.2
10 AP	304.0	255.8	84.1
20 AP	300.3	249.9	83.2

release plateau is observable in the coated samples, which might be a result of the activation of the Li_2MnO_3 in the bulk since the initial cycle was tested under 1/20 C which allows for sufficient diffusion. The charge capacity of the pristine HENMC, however, still shows noticeably more oxygen release as shown in Fig. 5c. For a pristine HENMC, the discharge capacity, in theory, mostly originates from the voltage above 3.0 V, considering the voltage window of Ni^{4+} to Ni^{2+}(4.0 V) and lithium insertion into MnO_2 (3.5 V). Therefore, in the pristine HENMC, very limited discharge capacity is expected to originate from the voltage below 3.0 V, as shown in Fig. 4c. However, we can also

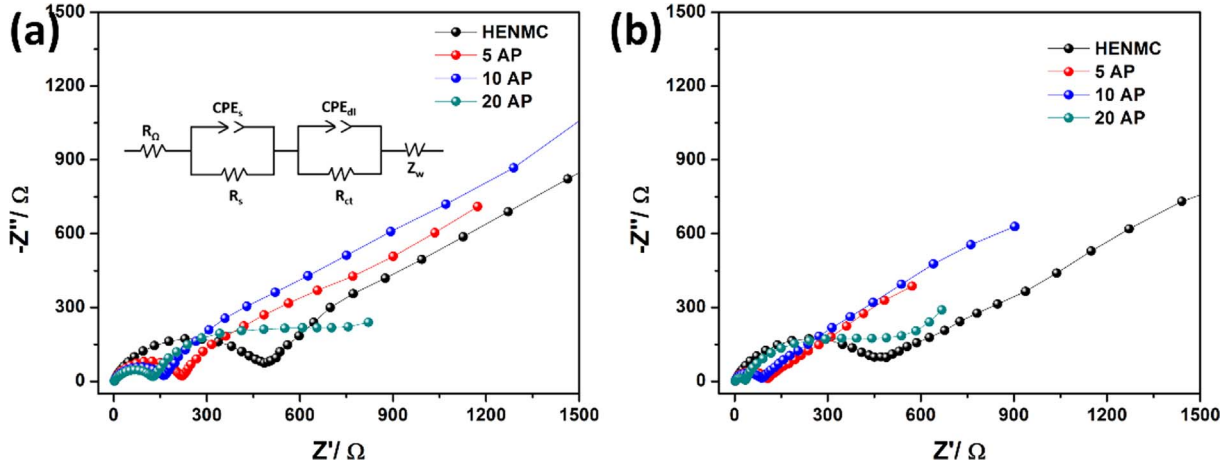

Fig. 6. EIS profiles of the samples (a) after initial charge and (b) after 6th charge (inset: A simulated equivalent circuit).

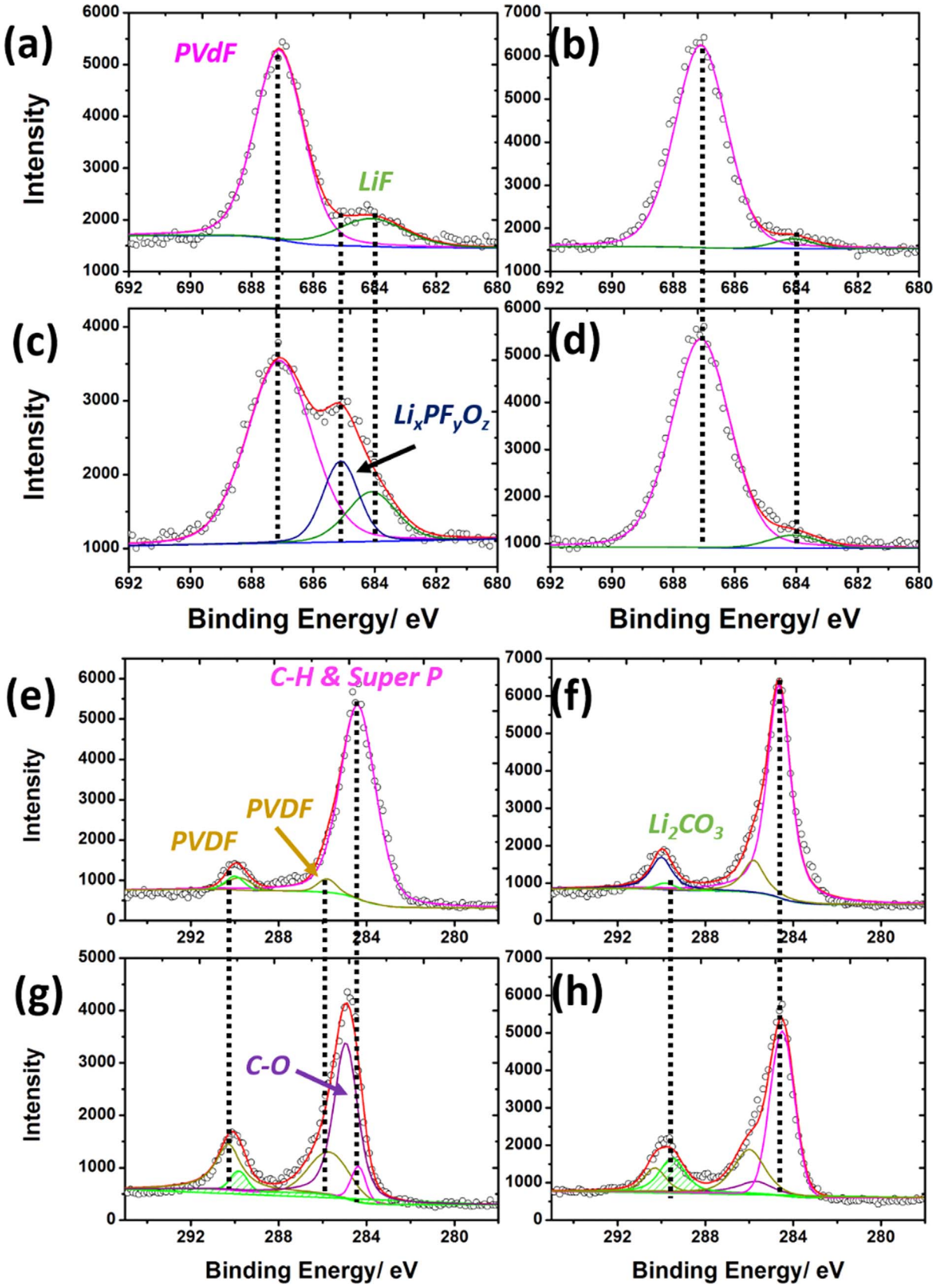

Fig. 7. XPS results of F 1 s of (a) Pristine HENMC electrode (b) HENMC-20AP electrode (c) Cycled pristine HENMC electrode (d) Cycled HENMC-20AP electrode and XPS results of C 1s of (e) Pristine HENMC electrode (f) HENMC-20AP electrode (g) Cycled pristine HENMC electrode (h) Cycled HENMC-20AP electrode.

observe that the higher initial discharge capacities of coated samples mainly come from the voltage below 3.0 V. The 20AP sample shows highest capacity below 3.0 V but obviously dropped capacity in the voltage range of 3.0–3.5 V. This phenomenon is in consistent with the CV curves and it indicates that the formation of MnO_2 has been suppressed and there was less Li insertion into MnO_2. This difference

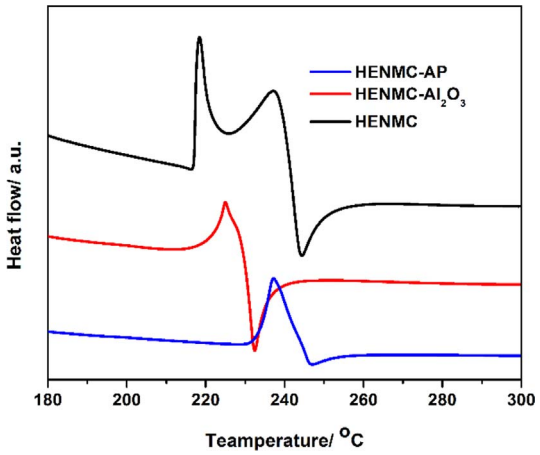

Fig. 8. DSC curves of pristine HENMC, HENMC-Al_2O_3 and HENMC-AP tested under N_2.

becomes more apparent in the charge/discharge curves of the 40th cycle. Voltage drop can be observed in all of the samples, and it is likely that such treatment is not effective towards the voltage drop suppression within short cycling. Nevertheless, the discharge capacities of 5 AP and 10 AP below 3.0 V are higher than that of the pristine HENMC. The above observations indicate that the presence of AP coating can help exploit the electrochemical reactions that take place below 3.0 V. In theory, capacities below 3.0 V in HENMC system stem from several sources: 1) polarization of the electrochemical processes that are supposed to take place above 3.0 V; 2) lithium insertion into the spinel phase on the surface [33] and 3) oxygen reduction reaction (ORR) [36,37]. A tiny plateau at ~2.7 V can be observed in coated samples, this agrees well with previous findings that a new spinel phase has formed upon ALD treatment. Aside from this plateau, extra capacity has been obtained below 3.0 V. ORR in HENMC normally happens as the O_2 gas that was released during initial charging process is reduced during discharge [4,36,37]. The final product of the oxygen reduction reaction is Li_2CO_3, which is electrochemically inert and enables stable SEI [38–40].

In order to evaluate the effect of the oxygen release on the formation of the SEI layer, EIS measurements were conducted on the pristine HENMC and coated HENMC samples after initial charge and 6th charge as shown in Fig. 6. The simulated equivalent circuit is presented as an inset. The R_Ω stands for the Ohmic resistance arose from the electrolyte, separator and other components. The semi-circle in the high frequency range represents the lithium diffusion across the surface film, simulated as a resistor R_s and a constant phase element (CPE), the semi-circle in the medium frequency range shows the charge transfer reaction composed of a resistor R_{ct} and another CPE, the inclined line is interpreted as the finite length Warburg impedance. In this case, the value of R_s stands for the SEI resistance and the R_{ct} stands for the charge transfer resistance across the material surface. The R_s for each of the sample after initial charge and 6th charge has been listed in Table S1. It can be seen that the pristine HENMC has an R_s of 432.9 Ω, whereas AP coating has demonstrated effectiveness in decreasing this resistivity. The drop of SEI impedance reveals that the electrolyte decomposition is much less intense in coated samples. This can be explained as that the $AlPO_4$ shields the HENMC particles from direct contact with the electrolyte. On the other hand, it could be due to the suppressed oxygen release, since oxygen will facilitate the electrolyte decomposition and hydrolysis under very high voltage. The R_s values of these samples after the 6th charge show an apparent drop, as can be seen from the right column of Table S1. For pristine HENMC, the R_s has a slight decrease of about 20 Ω. However, this drop becomes much more obvious in the coated samples, in the 20 AP sample, the R_s value has dropped by 85%. The reason for the impedance drop in these samples can be presumably ascribed to a more stable and thin SEI and/or the transformation of AP into lithium conductive Li_3PO_4 and $LiAlO_2$ [12,41]. The 20 AP sample shows the lowest R_s, but its capacity is lower than the 5 AP and 10 AP sample. Furthermore, voltage fade was not effectively alleviated even though the charge transfer impedance was much lower. This has also been observed in the work of Wang et al. [41], where they reported the suppression of layered to spinel change through ALD-derived Al_2O_3 coating, but voltage decay was still observed. These phenomena can be tentatively ascribed to the lack of MnO_2 phase due to the missing of the Li_2MnO_3 phase. The lithiation voltage window of layered MnO_2 falls into the window where voltage fade happens.

The surface compositions of the pristine HENMC, HENMC-20AP, cycled pristine HENMC and cycled HENMC-20AP electrodes are analyzed using XPS. Fig. 7a-d illustrate the F 1s XPS spectra. It can be seen that in fresh samples, two types of fluorine, PVdF at 687.1 eV and metal fluorides (LiF and transition metal fluorides) at 684 eV are observed. In general, LiF is not expected in fresh samples, but due to the dehydrofluorination of PVdF according to reaction (1), HF is produced.

$$-CH_2 - CF_2- \rightarrow -CH{=}CF- + HF \quad (1)$$

The surface of HENMC, after exposure to HF, generates LiF [42]. Apparently, the coated sample shows less LiF even in fresh samples, indicating that the presence of $AlPO_4$ is capable of protecting the material surface. Furthermore, after cycling, the surface F 1s XPS spectrum of pristine HENMC can be deconvoluted into three components, with an extra peak at 685.1 eV, this peak is generally assigned to $Li_xPF_y/Li_xPF_yO_z$, which are the main hydrolysis products of $LiPF_6$

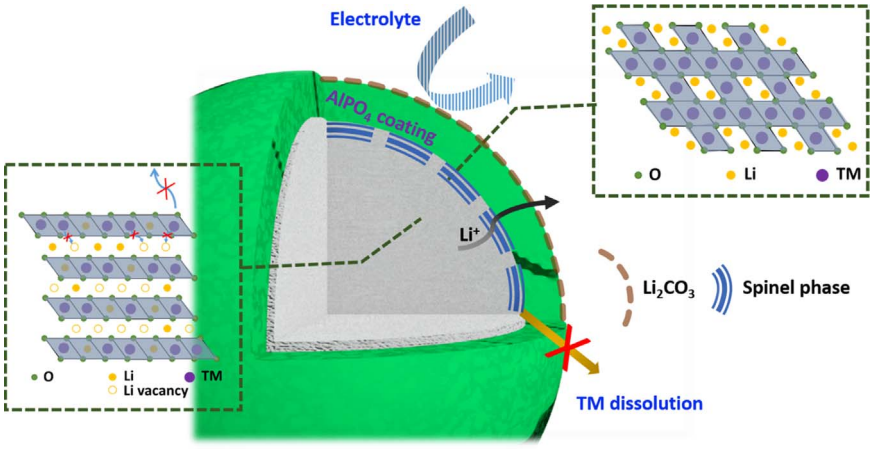

Fig. 9. Schematic illustration of the mechanisms of performance improvement by AP coating.

when exposed to O_2 and water [43,44]. The $Li_xPF_y/Li_xPF_yO_z$ peak cannot be observed in the coated cycled sample and the LiF in cycled pristine HENMC is also much more than that of the coated HENMC, indicating that the coating can effectively prevent the decomposition of the electrolyte upon cycling, especially when there is excessive oxygen generated in HENMC material.

The C 1s XPS spectra of the same samples were also studied. In the C 1s XPS, several peaks corresponding to the C-F and C-H bonds in PVdF, the C-C bonds in super P conductive agent and a small amount of Li_2CO_3 can be observed in the fresh electrodes [45]. However, after cycling, the pristine HENMC electrode shows a sharp peak of C-O single bond at the binding energy of 285.1 eV. In addition, the contribution from the super P conductive agent has dropped significantly in this sample, indicating that the surface has been covered by a very thick layer of electrolyte decomposition compounds. Since C-O bonds are normally assigned to species such as ether that are unfavorable SEI components due to their instability and insulating nature [46,47], we can conclude that the capacity fade of pristine HENMC is also closely related to the build-up of surface impedance. On the other hand, the coated HENMC, after cycling, shows much less C-O single bond, but the Li_2CO_3 peak turns out to be much higher than that of the pristine HENMC, this observation confirms our previous assumption that the decreasing impedance upon cycling in coated samples is because of Li_2CO_3 that helps create a more stable and robust SEI [40].

In addition, $AlPO_4$ coating is reported to be capable of enhancing the thermal resistivity of carbon nanotubes [48], we conducted DSC of charged pristine HENMC and AP coated HENMC was also conducted. Since Al_2O_3 is the most widely used ALD derived coating, a sample with Al_2O_3 coating was also studied as a reference. It can be seen from Fig. 8, the pristine HENMC shows two exothermal peaks, indicating that the dissociation of the HENMC was a two-step process. The first peak is normally assigned to the solvent decomposition and the second peak is supposed to originate from the cathode material phase change and the electrolyte oxidation [49]. The onset decomposing temperature was about 219 °C, whereas the Al_2O_3 coated sample shows a slightly higher onset temperature was 223 °C. However, AP coated sample shows significant improvement and the onset temperature was 237 °C, which is much higher than those of the pristine HENMC and Al_2O_3 coated HENMC. The thermal stability improvement of $AlPO_4$ coating can be ascribed to the high thermal stability of phosphate, thus proving that ALD-derived $AlPO_4$ is also a superior coating material in retaining the thermal stability of charged HENMC.

To better clarify the mechanism of the performance improvement by AP coating, we have shown a schematic diagram in Fig. 9. ALD process generates a spinel phase on the outer part of the material that enables fast Li^+ ion transportation, this differs from the cation migration caused phase which is due to lithium vacancies in the lithium layers. The AP coating protects the surface of HENMC from metal dissolution by shielding the particles from direct contact with the electrolyte. More importantly, the continuous oxygen release was suppressed so that the oxidation decomposition of the electrolyte under high voltage is also suppressed. Furthermore, the plausible oxygen reduction reaction that happens below 3.0 V has helped create a robust SEI with more Li_2CO_3, which also demonstrates increasing performance and over 100% CE within the first several cycles.

4. Conclusion

We have successfully used ALD to coat the HENMC cathode material with aluminum phosphate. This coating layer has demonstrated effective protection of the cathode material against the attack from the electrolyte. ALD process can slightly reduce the material surface and convert the Li_2MnO_3 to a spinel-like phase, and the oxygen release during initial charge can be effectively controlled. The initial coulombic efficiency can be significantly improved with the presence of the coating. Oxygen reduction reaction was more intense in the coated samples, it helped create a more robust SEI layer, so that the performance of the coated samples show significant improvement. Besides, AP coated HENMC has demonstrated much better thermal stability than Al_2O_3 coated HENMC and pristine HENMC, making it a promising candidate for the surface coating modification of HENMC since oxygen release may lead to severe thermal instability issues.

Acknowledgements

This research was supported by the Natural Science and Engineering Research Council of Canada (NSERC), General Motors R & D Center at Warren, US, the Canada Research Chair Program (CRC), the Canada Foundation for Innovation (CFI), Canadian Light Source (CLS) at the University of Saskatchewan, and the University of Western Ontario (UWO). Dr. Jian Liu is grateful to the financial support from NSERC Postdoctoral Fellowship Program. The authors are indebted to the help from Dr. Peng Lu on XPS.

Appendix A. Supplementary material

Supplementary data associated with this article can be found in the online version at doi:10.1016/j.nanoen.2017.02.015.

References

[1] P. Yan, J. Zheng, J. Xiao, C.-M. Wang, J.-G. Zhang, Front. Energy Res. 3 (2015) 26.
[2] H. Yu, H. Zhou, J. Phys. Chem. Lett. 4 (2013) 1268–1280.
[3] J. Rana, M. Stan, R. Kloepsch, J. Li, G. Schumacher, E. Welter, I. Zizak, J. Banhart, M. Winter, Adv. Energy Mater. 4 (2014) (1300998-130109).
[4] N. Yabuuchi, K. Yoshii, S.T. Myung, I. Nakai, S. Komaba, J. Am. Chem. Soc. 133 (2011) 4404–4419.
[5] P. Yan, L. Xiao, J. Zheng, Y. Zhou, Y. He, X. Zu, S.X. Mao, J. Xiao, F. Gao, J.-G. Zhang, C.-M. Wang, Chem. Mater. 27 (2015) 975–982.
[6] Y. Wu, C. Ma, J. Yang, Z. Li, L.F. Allard, C. Liang, M. Chi, J. Mater. Chem. A 3 (2015) 5385–5391.
[7] N. Dupre, M. Cuisinier, E. Legall, D. War, D. Guyomard, J. Power Sources 299 (2015) 231–240.
[8] K.-W. Nam, S.-M. Bak, E. Hu, X. Yu, Y. Zhou, X. Wang, L. Wu, Y. Zhu, K.-Y. Chung, X.-Q. Yang, Adv. Funct. Mater. 23 (2013) 1047–1063.
[9] S.-M. Bak, K.-W. Nam, W. Chang, X. Yu, E. Hu, S. Hwang, E.A. Stach, K.-B. Kim, K.Y. Chung, X.-Q. Yang, Chem. Mater. 25 (2013) 337–351.
[10] J. Zheng, M. Gu, J. Xiao, B.J. Polzin, P. Yan, X. Chen, C. Wang, J.-G. Zhang, Chem. Mater. 26 (2014) 6320–6327.
[11] Z. Wang, E. Liu, C. He, C. Shi, J. Li, N. Zhao, J. Power Sources 236 (2013) 25–32.
[12] Y. Wu, A. Vadivel Murugan, A. Manthiram, J. Electrochem. Soc. 155 (2008) A635–A641.
[13] A. Mauger, C. Julien, Ionics 20 (2014) 751–787.
[14] H. Liu, C. Chen, C. Du, X. He, G. Yin, B. Song, P. Zuo, X. Cheng, Y. Ma, Y. Gao, J. Mater. Chem. A 3 (2015) 2634–2641.
[15] Y.S. Jung, A.S. Cavanagh, L.A. Riley, S.H. Kang, A.C. Dillon, M.D. Groner, S.M. George, S.H. Lee, Adv. Mater. 22 (2010) 2172–2176.
[16] X. Meng, X.Q. Yang, X. Sun, Adv. Mater. 24 (2012) 3589–3615.
[17] J.S. Park, X. Meng, J.W. Elam, S. Hao, C. Wolverton, C. Kim, J. Cabana, Chem. Mater. 26 (2014) 3128–3134.
[18] X. Li, J. Liu, X. Meng, Y. Tang, M.N. Banis, J. Yang, Y. Hu, R. Li, M. Cai, X. Sun, J. Power Sources 247 (2014) 57–69.
[19] X. Li, J. Liu, M.N. Banis, A. Lushington, R. Li, M. Cai, X. Sun, Energy Environ. Sci. 7 (2014) 768.
[20] J. Liu, X. Sun, Nanotechnology 26 (2015) 024001–024014.
[21] J. Cho, T.-G. Kim, C. Kim, J.-G. Lee, Y.-W. Kim, B. Park, J. Power Sources 146 (2005) 58–64.
[22] A.T. Appapillai, A.N. Mansour, J. Cho, Y. Shao-Horn, Chem. Mater. 19 (2007) 5748–5757.
[23] B. Kim, C. Kim, T.-G. Kim, D. Ahn, B. Park, J. Electrochem. Soc. 153 (2006) A1773–A1777.
[24] J.-G. Lee, B. Kim, J. Cho, Y.-W. Kim, B. Park, J. Electrochem. Soc. 151 (2004) A801–A805.
[25] C.H. Shen, Q. Wang, F. Fu, L. Huang, Z. Lin, S.Y. Shen, H. Su, X.M. Zheng, B.B. Xu, J.T. Li, S.G. Sun, A.C.S. Appl, Mater. Interfaces 6 (2014) 5516–5524.
[26] S.P. Cramer, F.M.F. Degroot, Y. Ma, C.T. Chen, F. Sette, C.A. Kipke, D.M. Eichhorn, M.K. Chan, W.H. Armstrong, E. Libby, G. Christou, S. Brooker, V. Mckee, O.C. Mullins, J.C. Fuggle, J. Am. Chem. Soc. 113 (1991) 7937–7940.
[27] R.M. Qiao, T. Chin, S.J. Harris, S.S. Yan, W.L. Yang, Curr. Appl. Phys. 13 (2013) 544–548.
[28] A.J. Achkar, T.Z. Regier, E.J. Monkman, K.M. Shen, D.G. Hawthorn, Sci. Rep. 1 (2011) 182–188.
[29] L. Guo, N. Zhao, J. Li, C. He, C. Shi, E. Liu, ACS Appl. Mater. Interfaces 7 (2015)

391–399.
[30] Q. Xia, X. Zhao, M. Xu, Z. Ding, J. Liu, L. Chen, D.G. Ivey, W. Wei, J. Mater. Chem. A 3 (2015) 3995–4003.
[31] Y. Cho, S. Lee, Y. Lee, T. Hong, J. Cho, Adv. Energy Mater. 1 (2011) 821–828.
[32] Y.K. Sun, M.J. Lee, C.S. Yoon, J. Hassoun, K. Amine, B. Scrosati, Adv. Mater. 24 (2012) 1192–1196.
[33] J. Zheng, P. Xu, M. Gu, J. Xiao, N.D. Browning, P. Yan, C. Wang, J.-G. Zhang, Chem. Mater. 27 (2015) 1381–1390.
[34] P. Yan, A. Nie, J. Zheng, Y. Zhou, D. Lu, X. Zhang, R. Xu, I. Belharouak, X. Zu, J. Xiao, K. Amine, J. Liu, F. Gao, R. Shahbazian-Yassar, J.G. Zhang, C.M. Wang, Nano. Lett. 15 (2015) 514–522.
[35] M. Sathiya, A.M. Abakumov, D. Foix, G. Rousse, K. Ramesha, M. Saubanere, M.L. Doublet, H. Vezin, C.P. Laisa, A.S. Prakash, D. Gonbeau, G. VanTendeloo, J.M. Tarascon, Nat. Mater. 14 (2015) 230–238.
[36] H. Koga, L. Croguennec, M. Ménétrier, P. Mannessiez, F. Weill, C. Delmas, J. Power Sources 236 (2013) 250–258.
[37] H. Koga, L. Croguennec, M. Menetrier, K. Douhil, S. Belin, L. Bourgeois, E. Suard, F. Weill, C. Delmas, J. Electrochem. Soc. 160 (2013) A786–A792.
[38] J.S. Shin, C.H. Han, U.H. Jung, S.I. Lee, H.J. Kim, K. Kim, J. Power Sources 109 (2002) 47–52.
[39] B.R. Wu, Y.H. Ren, D.B. Mu, X.J. Liu, G.C. Yang, F. Wu, RSC Adv. 4 (2014) 10196–10203.
[40] C. Yogi, D. Takamatsu, K. Yamanaka, H. Arai, Y. Uchimoto, K. Kojima, I. Watanabe, T. Ohta, Z. Ogumi, J. Power Sources 248 (2014) 994–999.
[41] P. Verma, P. Maire, P. Novák, Electrochim. Acta 55 (2010) 6332–6341.
[42] P. Yan, J. Zheng, X. Zhang, R. Xu, K. Amine, J. Xiao, J.-G. Zhang, C.-M. Wang, Chem. Mater. 28 (2016) 857–863.
[43] Y.-C. Lu, A.N. Mansour, N. Yabuuchi, Y. Shao-Horn, Chem. Mater. 21 (2009) 4408–4424.
[44] T. Eriksson, A.M. Andersson, C. Gejke, T. Gustafsson, J.O. Thomas, Langmuir 18 (2002) 3609–3619.
[45] T. Eriksson, A.M. Andersson, A.G. Bishop, C. Gejke, T. r. Gustafsson, J.O. Thomas, J. Electrochem. Soc. 149 (2002) A69–A78.
[46] L. Yang, B.L. Lucht, Electrochem. Solid St. 12 (2009) A229–A231.
[47] H. Bouayad, Z. Wang, N. Dupré, R. Dedryvère, D. Foix, S. Franger, J.F. Martin, L. Boutafa, S. Patoux, D. Gonbeau, D. Guyomard, J. Phys. Chem. C 118 (2014) 4634–4648.
[48] L. Yang, B. Ravdel, B.L. Lucht, Electrochem. Solid St. 13 (2010) A95–A97.
[49] J. Liu, Y.J. Tang, B.W. Xiao, T.K. Sham, R.Y. Li, X.L. Sun, RSC Adv. 3 (2013) 4492–4495.

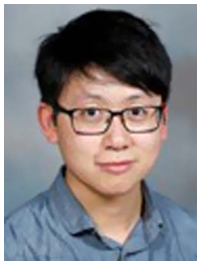

Biwei Xiao has just finished his Ph.D. degree in Prof. Xueliang (Andy) Sun's group at the University of Western Ontario. He earned his bachelor of engineering degree from Sichuan University (China) in 2011. His research interests are associated with the synthesis, modification and mechanism study of cathode materials for lithium-ion batteries, atomic layer deposition, synchrotron radiation technique and carbonaceous materials.

Biqiong Wang is currently a Ph. D. candidate in Prof. Xueliang (Andy) Sun's Nanomaterials and Energy Group at Western University, Canada. She received her Bachelor degree in Materials Science in 2012 at the City University of Hong Kong. Her research interests are associated with the application of atomic layer deposition in all-solid-state batteries. She is also co-supervised by Prof. T. K. Sham from Chemistry Department in Western University. Part of her work is related to the study of energy materials via synchrotron radiation.

Jian Liu is an Assistant Professor at the University of British Columbia (UBC Okanagan campus), Canada. Dr. Liu received his Ph.D. in materials science in 2013 from the University of Western Ontario (Canada), and worked as a NSERC Postdoctoral Fellow at Lawrence Berkeley National Laboratory (USA) and Pacific Northwest National Laboratory (USA) before joining UBC in Jan 2017. His current research interests lie in advanced nanofabrication techniques, key materials for Li-ion and next-generation batteries, and interface control and understanding in complex energy systems.

Karthikeyan Kaliyappan received Bachelor of technology (B.Tech, 2005) and Master of technology (M.Tech, 2007) in Electrochemical Engineering from Central Electrochemical Research Institute, India. After completing masters, he worked as Junior Research Fellow in materials technology division, Central Power Research Institute, India from October 2007 to February 2009. He earned Ph.D. at Chonnam National University, South Korea in Advanced Chemicals and Engineering (2013). He is currently working as a postdoctoral fellow at the University of Waterloo, Waterloo, Canada. His current fields of interests are developing high energy density materials for energy storage devices including Li-ion and Na-ion batteries. He also worked on the fabrication of high performance lithium ion capacitors.

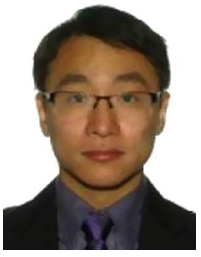

Dr. Qian Sun is a postdoctoral fellow in Prof. Xueliang (Andy) Sun's Group at the University of Western Ontario, Canada. He received his B.S. degree in Chemistry in 2006, M.S. degree in Physical Chemistry in 2009, and Ph.D. degree in Applied Chemistry in 2013 at Fudan University, China, under the supervision of Prof. Dr. Zheng-Wen Fu on the study of Li-/Na-ion batteries and Na-air batteries. He joined Prof. Sun's group in 2013 and his current research interests focus on Na-air, Na-S, and Na-ion batteries as well as solid-state Li/Na batteries.

Yulong Liu is currently a Ph.D. candidate in Prof. Xueliang (Andy) Sun' Nanomaterials and Energy Group at the University of Western Ontario, Canada. He received his Bachelor degree from Central South University, China, in 2010, and Master degree in 2013. His research interests include nanomaterials for lithium ion batteries, especially $LiFePO_4$ (in collaboration with Phostech Lithium Inc.), and the development of solid state batteries.

Gayatri Dadheech is a Staff Researcher at General Motors Global Research and Development Center for last 17 years. She has been working on materials science and engineering for various automotive applications including the electrochemical energy storage and conversion. She led the electrode and bipolar plate coatings for 13 years in GM's Fuel Cell Program. She has numerous research disclosures, trade secrets, publications and 75 US patents granted and 30+ patent pending. Prior to GM she was a postdoctoral fellow at the University of Detroit Mercy.

Michael P. Balogh is currently a Technical Fellow at General Motors Research and Development Center working in the Chemical and Materials Systems Laboratory. Mike joined the GM Research laboratories in 1983 after graduating from the University of Michigan with a BS degree in Chemistry. In 1993, he received a MS degree in Materials Science and Engineering from Wayne State University. His research interests are materials microstructure characterization using transmission electron microscopy (TEM), scanning TEM (STEM), x-ray diffraction (XRD) and focused ion beam/scanning electron microscopy (FIB/SEM). His characterization experience has involved a wide range of materials including polymers, metals, ceramics, catalysts, semiconductors, electronic materials, thin films, coatings, fuel cell materials, hydrogen storage materials and battery materials. Mike has coauthored over 50 papers and holds over 20 patents.

Li Yang received his B.E. and M.E. in Chemical Engineering from Northwestern Polytechnic University (Xi'an, China) in the year 1997 and 2000. He obtained Ph.D. degree in Organic Chemistry at the University of Rhode Island in 2009 under the guidance of Prof. Brett Lucht. He joined Dr. John Kerr's group at the Lawrence Berkeley National Laboratory as a postdoctoral fellow from 2009 to 2011. In 2011, he joined the General Motors Global Research and Development Center as a Senior Researcher. His research is focused on the development of liquid and polymeric electrolytes for Li-ion batteries, Li-S batteries and other high energy density storage technologies.

T.K. Sham is a Distinguished University Professor and a Canada Research Chair in Materials and Synchrotron Radiation at the University of Western Ontario. He obtained his PhD from the University of Western Ontario (1975) with a BSc from the Chinese University of Hong Kong. He joined the Chemistry Department at Brookhaven National Laboratory in 1977 and returned to Western in 1988. He is presently the Director of the Soochow-Western Center for Synchrotron Radiation, a Fellow of the Royal Society of Canada and an Officer of the Order of Canada. Dr. Sham's expertise are nanomaterial synthesis, surface and interface, X-ray absorption related spectroscopy and microscopy. His recently focus is nanostructure phase transition, assembly of nanocomposites, in situ/in operando studies of energy materials and devices. X-ray excited optical luminescence in the energy and time domain, nanomaterials for drug delivery, and micro-beam analysis of cultural and heritage materials.

Ruying Li is a research engineer in Prof. Andy Xueliang Sun's group at the University of Western Ontario, Canada. She received her master degree in materials chemistry in 1999 from the University of Manchester, UK. Then she worked as a research assistant at the University of British Columbia, Canada and L'Institut National de la Recherche Scientifique (INRS), Canada. Her current research interests are focused on advanced materials and characterization for electrochemical energy storage and conversion, including electrocatalysis in fuel cells and electrodes in lithium batteries.

Dr. Mei Cai is a General Motors technical fellow and the manager of Energy Storage Materials Group at General Motors Global Research and Development Center. Dr. Cai received her Ph.D. in Chemical Engineering in 1999 from Wayne State University, Detroit, Michigan and has been with GM for 20 years. She has extensive experience in many of the advanced energy materials research area, including fuel cells, gaseous fuel storage, batteries, and capacitors. Her current research interests are focused on synthesis and processing of nanostructured materials, nanocomposite materials, and their applications in automotive clean energy areas.

Xueliang (Andy) Sun is a Canada Research Chair in Development of Nanomaterials for Clean Energy, Fellow of the Royal Society of Canada and Canadian Academy of Engineering and Full Professor at the University of Western Ontario, Canada. Dr. Sun received his Ph.D. in materials chemistry in 1999 from the University of Manchester, UK, which he followed up by working as a postdoctoral fellow at the University of British Columbia, Canada and as a Research Associate at L'Institut National de la Recherche Scientifique (INRS), Canada. His current research interests are focused on advanced materials for electrochemical energy storage and conversion, including electrocatalysis in fuel cells and electrodes in lithium-ion batteries and metal–air batteries.